

# A Low-Power Backscatter Modulation System Communicating Across Tens of Meters With Standards-Compliant Wi-Fi Transceivers

Po-Han Peter Wang<sup>ID</sup>, *Member, IEEE*, Chi Zhang, Hongsen Yang, *Graduate Student Member, IEEE*, Manideep Dunna, Dinesh Bharadia, and Patrick P. Mercier<sup>ID</sup>, *Senior Member, IEEE*

**Abstract**—This article presents the first integrated circuit designed to enable low-power backscatter communication with commodity Wi-Fi transceivers. The developed chip operates by receiving a series of packets generated from a Wi-Fi access point (AP), which feeds into a low-power energy-detecting wake-up receiver that determines when backscatter communication should commence. Then, the Wi-Fi AP sends an additional packet that is intended to be backscatter modulated. To accomplish this, the antenna receiving the incident Wi-Fi packet is terminated by a dynamically varying collection of complex impedances via a crystal-stabilized multi-phase local oscillator driven by a single-sideband (SSB) mixer, which ultimately performs SSB quadrature phase shift-keying (QPSK) modulation with frequency-translation to a separate Wi-Fi channel for reception by a second Wi-Fi AP. Implemented in 65-nm CMOS, the downlink wake-up receiver consumes  $2.8 \mu\text{W}$  and achieves a sensitivity of  $-42.5 \text{ dBm}$ , which is good enough for  $>30 \text{ m}$  wake-up range, while the backscattering uplink consumes  $28 \mu\text{W}$  and achieves  $17 \text{ dB}$  of image rejection. Wireless tests reveal a range of  $21 \text{ m}$  when the developed IC is placed symmetrically between Wi-Fi access points (APs), and a range of  $>90 \text{ m}$  when the developed IC is placed within  $1 \text{ m}$  of the transmitting Wi-Fi AP.

**Index Terms**—2.4-GHz band, backscatter communication, image rejection, Internet-of-Things (IoT), low-power wireless, RFID, single-sideband (SSB), wake-up radios, wake-up receivers (WuRXs), Wi-Fi.

## I. INTRODUCTION

**M**OST Internet of Things (IoT) devices for use in smart homes, environmental monitoring, industrial IoT, and

Manuscript received May 15, 2020; revised August 31, 2020; accepted September 1, 2020. Date of publication September 24, 2020; date of current version October 23, 2020. This article was approved by Associate Editor Edoardo Charbon. This work was supported in part by the National Science Foundation under Grant 1923902. (Corresponding authors: Po-Han Peter Wang; Patrick P. Mercier.)

Po-Han Peter Wang was with the Department of Electrical and Computer Engineering, University of California at San Diego, La Jolla, CA 92093 USA. He is now with Broadcom Inc., San Diego, CA 92127 USA (e-mail: po-han-peter.wang@broadcom.com).

Chi Zhang was with the Department of Electrical and Computer Engineering, University of California at San Diego, La Jolla, CA 92093 USA. He is now with Google LLC, San Diego, CA 92121 USA.

Hongsen Yang was with the Department of Electrical and Computer Engineering, University of California at San Diego, La Jolla, CA 92093 USA. He is now with Aethercomm, Inc., Carlsbad, CA 92010 USA.

Manideep Dunna, Dinesh Bharadia, and Patrick P. Mercier are with the Department of Electrical and Computer Engineering, University of California at San Diego, La Jolla, CA 92093 USA (e-mail: dineshb@ucsd.edu; pmercier@ucsd.edu).

Color versions of one or more of the figures in this article are available online at <http://ieeexplore.ieee.org>.

Digital Object Identifier 10.1109/JSSC.2020.3023956

0018-9200 © 2020 IEEE. Personal use is permitted, but republication/redistribution requires IEEE permission. See <https://www.ieee.org/publications/rights/index.html> for more information.

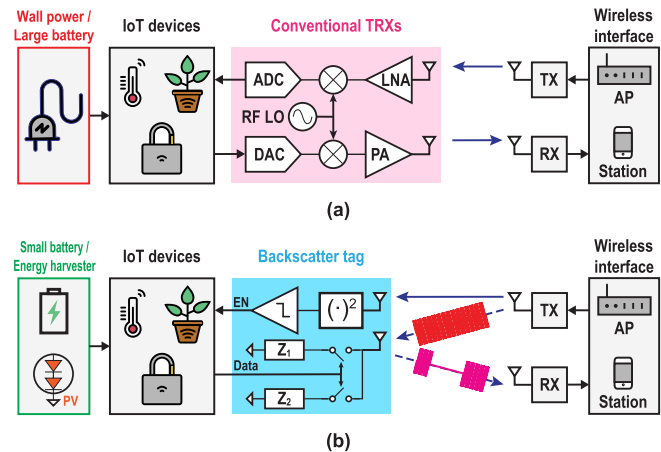


Fig. 1. Wireless communication using (a) conventional high power transceivers and (b) low power backscatter tag.

beyond require wireless connectivity. To keep costs low, it is generally desired to leverage existing wireless network infrastructure as much as possible; otherwise, deploying custom access points can get prohibitively expensive. In smart home and office environments, there is only one pervasive wireless network infrastructure in place today: Wi-Fi. As a result, most IoT devices used in these applications don't have a choice: they connect to the internet via Wi-Fi.

However, Wi-Fi is by no means a low-power approach to enable wireless communications. Conventional Wi-Fi transceivers require 10s to 100s of mW of active power from radio frequency (RF) blocks such as low noise amplifiers (LNAs), local oscillator (LO) frequency generation and stabilization, and power amplifiers (PAs), in part due to strict performance demands imposed by the IEEE 802.11-based standards. As a result, nearly all current Wi-Fi compatible IoT devices require either wall power, or large and/or frequently re-charged batteries as depicted in Fig. 1(a).

While other standards with lower standards-based performance requirements, such as Bluetooth low energy (BLE), may achieve very low average power ( $\ll 1 \text{ mW}$ ) via duty-cycling at the expense of throughput and latency, very small coin cell batteries or energy harvesters still cannot be used due to relatively high peak power requirements (e.g., a few mW for BLE) [1], which therefore limits new products to certain minimum device sizes. More importantly, standards such as BLE do not have widely distributed infrastructure in most

homes, offices, or other environments, which makes rapid low-cost deployment difficult.

Instead of building an active modulator and transmitter, backscatter communication, where an incident wave to an antenna sees a time-varying impedance profile that creates a modulated reflected signal, can materially decrease the power needed to enable wireless communications at the IoT device level. The idea of using backscatter communications is not new: it is the main method of communication in radio frequency identification (RFID) systems, and has been used for military radar detection system since the 1960s [2]. However, recent works have shown that backscatter communication can be an effective solution to enable new class of miniaturized, battery-powered or energy-harvested IoT devices by replacing a conventional high power transceiver with a low power backscatter tag to establish communication with the wireless interface, as shown in Fig. 1(b) [3]–[14].

Perhaps the most popular technologies leveraging backscatter communications today are near-field communication (NFC) and RFID tags. As shown in Fig. 2(a), NFC tags, which are widely used in applications such as contactless payment systems and electronic keycards, use near-field inductive coupling between two coils to transmit data, which limits the operating range to within approximately 10 cm of the source; for this reason, NFC is not well suited for most IoT applications. However, because of its inductive coupling mechanism, NFC tags normally operate at 13.56 MHz and are resilient to RF interference. To enlarge communication range, RFID tags, which can be widely seen in applications such as high-way electronic toll system and inventory management system [4], use far-field radiative coupling for transmission [Fig. 2(b)]. Therefore, RFID tags normally operate at 0.4–2.4 GHz, and meters of communication range are achievable [3], [5]–[7]. Although this approach is suitable for IoT devices in terms of range and power, the following problems need to be addressed.

- 1) *Spectral Efficiency*: As will be shown in Section II, conventional RFID tags receive a continuous wave (CW) signal and reflect it with data modulation limited to amplitude-shift keying (ASK) or on-off-keying (OOK) only; these are not spectrally efficient. Techniques that can modulate the reflected wave with higher order of modulation such as QPSK are of interest.
- 2) *Interference Resiliency*: As mentioned above, since the downlink incident wave is a CW signal, and the uplink reflected wave is a ASK/OOK signal, RFID tags are very susceptible to RF interference. To solve this issue, normally the direction and location of the CW source (e.g., RFID readers) are optimized, for example, inside a warehouse using an RFID inventory management system, which is not practical for mass IoT devices coexistence at home or in urban areas. Techniques that can use signals with interference-resilient modulation such as phase shift-keying (PSK) with direct-sequence spread spectrum (DSSS) (e.g., 802.11b Wi-Fi) would be beneficial.
- 3) *Standard Compatibility and Low-Cost Deployment*: To generate a CW incident wave and be able to demodulate the reflected signal, a dedicated RFID reader is

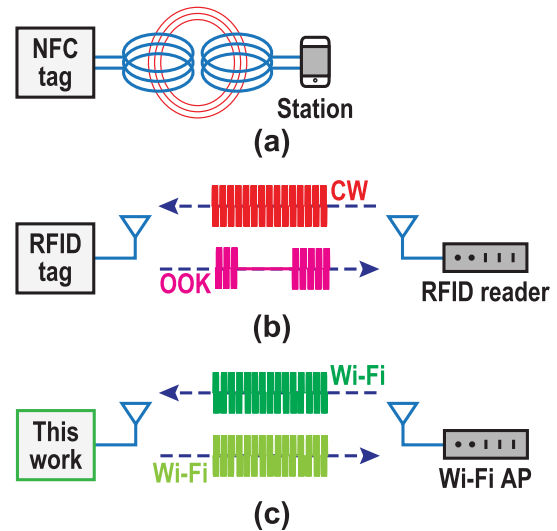


Fig. 2. Technologies using backscatter communication. (a) NFC tags. (b) RFID tags. (c) Proposed Wi-Fi compatible backscatter tags.

required. However, this approach contradicts the target of cost-effective direct deployment that leverages well-established standards such as Wi-Fi.

To attempt to address these issues, this article presents an integrated circuit that can perform spectrally efficient QPSK backscatter modulation on top of standards-compliant Wi-Fi signals at low power, for reception by commodity Wi-Fi hardware as illustrated in Fig. 2(c) by: 1) waking up to carefully architected incident Wi-Fi compatible packets via an integrated  $2.8 \mu\text{W}$  energy-detecting wake-up receiver (WuRX); 2) modulating the phase of incident Wi-Fi signals and frequency-translating them to another Wi-Fi channel via a crystal-stabilized multiphase LO to enable clear and robust reception of protocol-compliant data; 3) utilizing an IQ mixer driving multi-phase-terminated backscatter switches to enable SSB QPSK modulation to a single adjacent Wi-Fi channel; and 4) receiving and decoding the tag data with a commercial Wi-Fi TRX by XOR-ing the original incident Wi-Fi data (via the cloud) and the received backscattered alteration.

This design was originally presented in [14]; this article provides significant additional system design and circuit implementation details. The proposed SSB backscatter modulation technique is presented in Section II, while Section III describes the proposed Wi-Fi-compliant backscatter solution. Section IV presents circuit implementation details, followed by measurement results in Section V. Finally, Section VI concludes this article.

## II. BACKSCATTER MODULATION APPROACHES

### A. Prior-Art Techniques

The most basic way to perform backscatter modulation is to modulate a single pole double throw (SPDT) switch, which connects the antenna to two different load impedances,  $Z_{L,1}$  and  $Z_{L,2}$ , typically via a transmission line [3], as depicted in Fig. 3(a). By alternatively selecting these two loads, which provides different reflection coefficients,  $\Gamma_{in,1}$  and  $\Gamma_{in,2}$  at the antenna interface, tag data can be modulated onto the reflected waves. If  $\Gamma_{in,1}$  and  $\Gamma_{in,2}$  have different magnitudes,

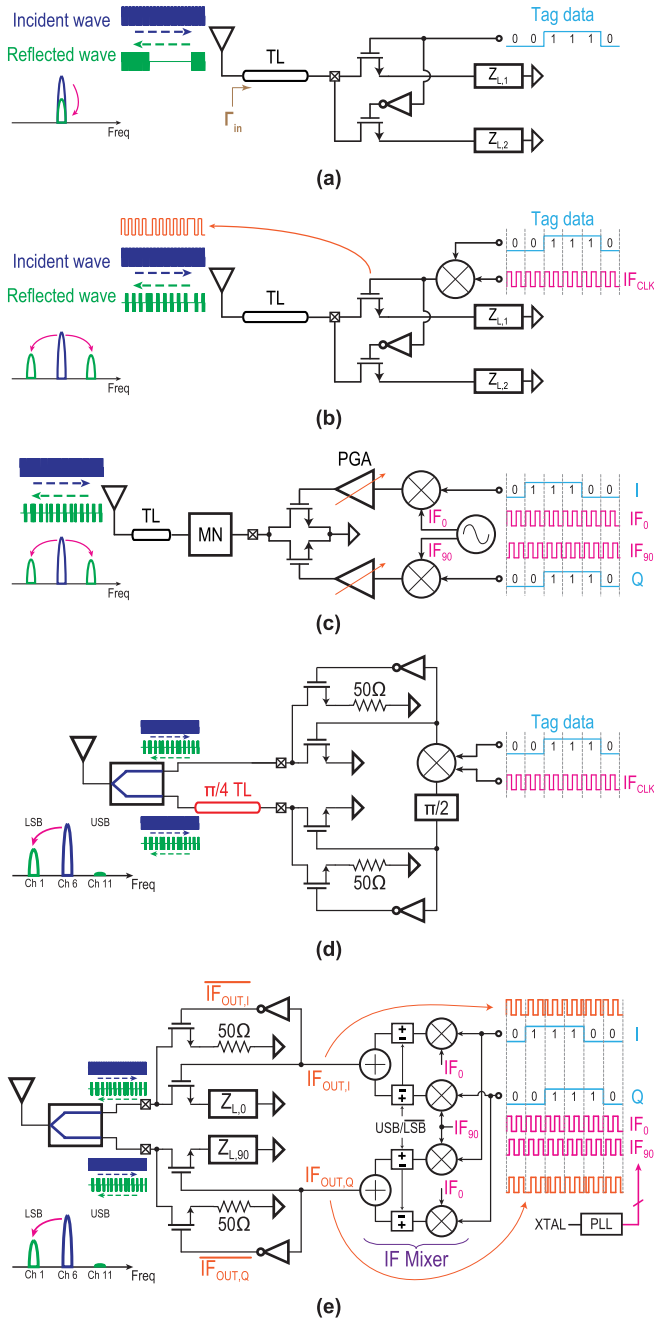


Fig. 3. Methods to perform ON-chip backscatter modulation. (a) Conventional frequency-overlapped OOK. (b) Frequency-translated BPSK. (c) Frequency-translated QPSK/QAM. (d) TL-based SSB BPSK. (e) Proposed TL-less programmable SSB QPSK approach.

an ASK or OOK modulation can be achieved [5], [6], [12]. For example, if  $Z_{L,1} = 50 \Omega$ , no reflection will occur and the incident wave will be fully absorbed, while if  $Z_{L,2} \neq 50 \Omega$ , for example, an open or short circuit, then incident power will be fully reflected, creating an effectively OOK-modulated backscatter signal. Although simple to implement, the ASK/OOK backscatter modulated signal is not spectrally efficient, nor is it robust to interference.

Instead of amplitude modulation, BPSK modulation, which theoretically requires lower signal-to-noise ratio (SNR) to demodulate, can be achieved if the real part of  $\Gamma_{in,1}$  and  $\Gamma_{in,2}$

are the same while the imaginary part is out of phase [3]. However, BPSK also has low spectral efficiency. Although 4-QAM modulation is achieved in [7] by connecting four distinct loads that provide four constellation points (i.e.,  $\Gamma_{in}$ ) on the Smith chart to the antenna via an SP4T switch, this approach highly depends on the accuracy of the  $RLC$  passives, and the requirement of inductors to not degrade the backscattering amplitude can increase the footprint/cost. More importantly, the incident signal is at the same frequency channel as the reflected signal and becomes a self-jammer, which makes signal separation/filtering difficult for the distal reader.

Since backscatter modulation is performed by passive switches, the frequency translation nature of a passive mixer can be leveraged to solve the self-jammer issue. As shown in Fig. 3(b), instead of driving the switches directly, the baseband data can be first mixed with an IF clock at frequency  $f_{IF}$ , which then frequency translates the backscattered signal to an alternate channel that is  $f_{IF}$  away from the incident signal. By selecting  $f_{IF}$  to be 10 s of MHz, a well-designed receiver can easily filter out the unwanted incident signal and demodulate the backscattered signal directly without any complicated and power hungry hardware for full-duplex radios [15]. In this scenario, BPSK modulation is achieved by alternating the phase of the IF clock directly [13].

To improve spectral efficiency while adopting frequency translation, an IF-based quadrature backscattering technique is proposed in [8], as shown in Fig. 3(c). Here, an I/Q quadrature mixer first up-converts the I/Q baseband data to IF, and drives the corresponding I/Q switches via programmable amplifiers (PGAs). The parallel resistance formed by the I/Q transistors in the triode region then provide QPSK modulated  $\Gamma_{in}$  with constant PGA gain, and up to 32-QAM with PGA gain control. However, this analog approach by modulating the transistor resistance highly depends on the transistor threshold voltage  $V_t$ , which makes PVT variation of concern, and is only effective when the incident signal is a single-tone sinusoidal wave, which prohibits the target to communicate with commodity Wi-Fi transceivers.

Since the frequency-translation technique in [8] and [13] only modulates one set of switches with the IF signal, the reflected signal has a frequency offset of  $\pm f_{IF}$  and creates a double sideband modulation, which is not spectrally efficient and may interfere with devices operating on other channels. To solve this issue, a transmission-line-based single sideband (SSB) backscatter technique is proposed in [11] and is depicted in Fig. 3(d). In this approach, one set of backscatter switches is driven by the IF data directly, while another set of switches (i.e., a quadrature path) is driven by the IF data with a  $\pi/2$  phase delay at IF. An extra transmission line that provides a  $\pi/4$  phase delay at RF is also inserted at the quadrature path, which provides a  $\pi/2$  total phase delay for the reflected signal (i.e.,  $\pi/4$  from incident direction and  $\pi/4$  from reflected direction). By summing up these two reflected signals via a power combiner, SSB backscattering can be achieved. However, this extra transmission line enlarges the tag footprint and makes this technique narrow band since the transmission line only offers the desired  $\pi/4$  over a narrow

range of frequencies. Moreover, this technique is only verified on a board level prototype with fixed IF phase delay, which can only backscatter to a fixed sideband channel.

### B. Proposed Technique

A transmission-line-less programmable SSB QPSK backscatter modulator is proposed based on a heterodyne transmitter approach as depicted in Fig. 3(e) [14]. The quadrature IF clocks are generated from a crystal-stabilized (and thus PVT-robust) PLL. The quadrature I/Q data is first up-converted to quadrature IF signals via two IF SSB mixers [16], and the quadrature IF signals then drive two sets of backscatter switches, respectively. To generate the required quadrature RF signals that mix with the quadrature IF signals for SSB modulation, two distinct loads that provide  $\pi/2$  phase difference in reflection coefficients (i.e.,  $Z_{L,0}$  and  $Z_{L,90}$ ) are connected to each set of the backscatter switches, respectively. By summing up these two backscattered signals via a power combiner, SSB backscattering can be achieved. In this design,  $Z_{L,0}$  is an open circuit which has  $\Gamma_{L,0} = e^{j \times 0^\circ}$ , while  $Z_{L,90} = -j \times 50$  and is realized by a 1.3 pF capacitor including parasitics at the operating 2.4 GHz band, which has  $\Gamma_{L,90} = e^{j \times -90^\circ}$ , respectively. Moreover, for the two 50  $\Omega$  paths, the 50  $\Omega$  termination is realized directly by the on-resistance of the switching transistor. The on-resistance of the switch that connects to the capacitor is  $\sim 2.5 \Omega$ .

Interestingly, the use of a capacitor to realize the  $\pi/2$  phase shift makes capacitor variation and therefore phase variation of concern. In fact, this phase variation causes the same issue as conventional image-rejection transceivers, where the RF LO I/Q mismatch results in sideband leakage and therefore lower image-rejection ratio (IRR). Since capacitor variation will only change the phase of  $\Gamma_{L,90}$  rather than the magnitude, the IRR is ideally dominated by the phase variation only and can be simplified as [17]

$$\text{IRR} \approx \frac{4}{\Delta\theta^2} \quad (1)$$

where  $\Delta\theta$  is phase difference and can be derived as

$$\begin{aligned} \Delta\theta &= \angle\Gamma_{L,90} - \left(-\frac{\pi}{2}\right) = \angle\left(\frac{Z_{L,90} - Z_0}{Z_{L,90} + Z_0}\right) + \frac{\pi}{2} \\ &= \angle\left(\frac{\frac{1}{j\omega C_L} - Z_0}{\frac{1}{j\omega C_L} + Z_0}\right) + \frac{\pi}{2} \\ &= 2 \tan^{-1}\left(\frac{1}{\omega C_L Z_0}\right) - \frac{\pi}{2} \end{aligned} \quad (2)$$

and  $Z_0$  is the transmission-line characteristic impedance,  $C_L$  is the capacitor for phase shifting, and  $\omega$  is the angular frequency, respectively. Assuming a target IRR of 20 dB, which is typical for a first-order image rejection mixer realized by passive *RCCR* network, the following equation can be derived to find the tolerable range of  $C_L$  by plugging (2) into (1)

$$\tan^{-1}\left(\frac{1}{\omega C_L Z_0}\right) = \frac{\pi}{4} \pm 0.1. \quad (3)$$

Assuming an ideal 50  $\Omega$   $Z_0$  and a 2.44-GHz operating frequency,  $C_L$  can vary between 1.1 and 1.6 pF, which is

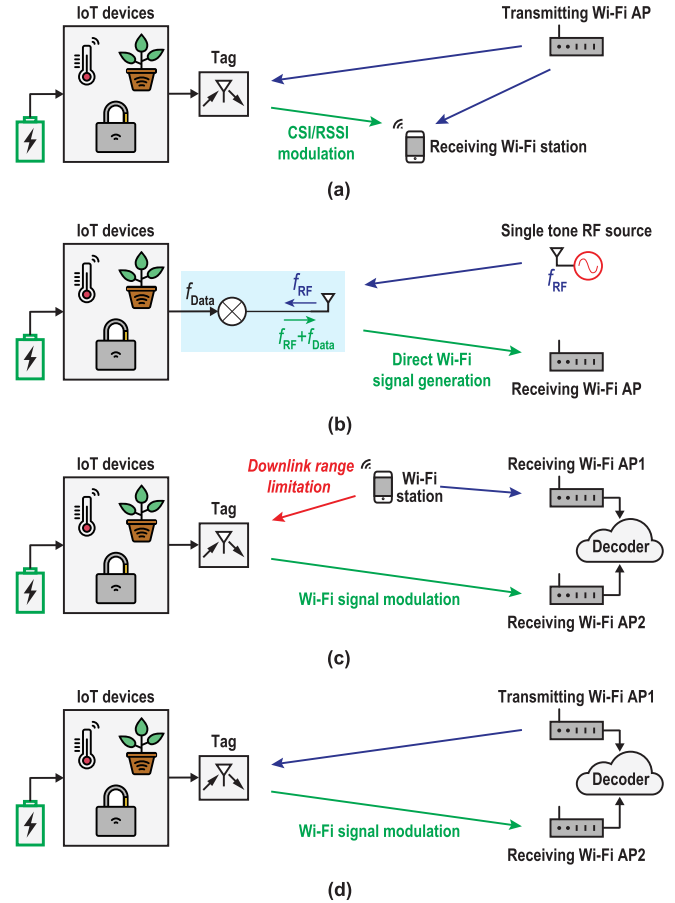


Fig. 4. Solutions to perform Wi-Fi compatible backscatter communication. (a) Wi-Fi backscatter via CSI/RSSI modulation. (b) Passive Wi-Fi via direct Wi-Fi signal generation. (c) Hitchhike via Wi-Fi signal modulation and cloud decoder but with downlink range limitation. (d) Proposed Hitchhike via Wi-Fi signal modulation and cloud decoder without downlink range limitation.

reasonable for a typical implementation even under severe variation.

It should be noted that alternative capacitors may be switched in to provide more precise phase differences as the channel frequency is programmed, which is another benefit provided by this ON-chip SSB technique compared to OFF-chip transmission-line approach. Moreover, by selecting the proper sign to the adder in the IF SSB mixer, either upper sideband (USB) or lower sideband (LSB) backscattering can be achieved.

## III. WI-FI COMPATIBLE BACKSCATTER COMMUNICATION

### A. Overall Requirements for Full Wi-Fi Compatibility

Baseline RFID systems require a CW signal to backscatter data onto—this requires a dedicated custom tone transmitter, which is not compatible with a low-cost rapid deployment strategy using commodity hardware. Instead, it is desired to have all incident signals come from a standards-compliant Wi-Fi transmitter, and backscatter signals that can be directly decoded by a standards-compliant Wi-Fi receiver. This requires not only a Wi-Fi compatible uplink (i.e., backscattering data from the tag to a Wi-Fi-compatible receiver), but also a Wi-Fi-compatible downlink, such that the backscattering tag knows precisely when to begin the

backscattering process. Most prior art literature cannot do this using only commodity Wi-Fi hardware, and none have demonstrated a low-power backscattering integrated circuit.

### B. Prior Art Techniques

The first Wi-Fi compatible solution proposed in the literature is called Wi-Fi Backscatter [9] and is depicted in Fig. 4(a). Here, a Wi-Fi access point (AP) transmits the signal to both the tag and the receiving Wi-Fi station, while the tag modulates the channel received signal strength indicator (RSSI) by absorbing and backscattering the signal alternately with the tag's data. This ASK-modulated signal (modulated in terms of RSSI) can be demodulated by the receiving Wi-Fi station via checking the channel state information (CSI) or RSSI, which are normally provided in state-of-the-art Wi-Fi chipsets. This approach is quite simple to implement and appears to meet all of the requirements stated in the prior section; however, this approach uses the entire Wi-Fi packet as a single bit, and therefore achieves very low data rate (100 s of bps). Moreover, the inherent lower sensitivity RSSI receiver from the standard chips along with ambient noise in the implemented system limited the range in [9] to only 0.65–2.1 m.

Another solution, called passive Wi-Fi, [10], was designed to address the issues of [9]. The overall approach is depicted in Fig. 4(b). Here, this design uses a conventional TX architecture to generate an IEEE 802.11b baseband signal directly, but instead of generating the power hungry RF LO locally, a single tone RF source provides the RF LO outside, and the Wi-Fi compatible packet is synthesized by combining the baseband signal with the incident LO via backscatter modulation through the antenna. Although this method can enable low power tag, only the uplink is Wi-Fi compatible while the downlink still requires custom hardware to generate the CW signal.

A solution to this issue called Hitchhike is proposed in [11] and can achieve Wi-Fi compatibility in both the downlink and the uplink. In this design, illustrated in Fig. 4(c), a Wi-Fi signal generated by a mobile phone creates the incident signal received by the IoT tag. The tag performs PSK-based modulation on each symbol of the incident wave, which creates a backscatter signal on a different channel for reception by a Wi-Fi access point (AP2 in this example). Meanwhile, the original un-disturbed Wi-Fi transmission from the mobile phone is received by another access point (AP1 in this example). Thus, AP1 has the original phone data, while AP2 has phone data that has been phase modulated by the IoT tag. By connecting the two APs through the cloud, both data are available to a decoder. This decoder employs a technique called codeword translation, described in more detail shortly, to decode the tag's data.

To make HitchHike work, there is only technically a need for one Wi-Fi transmitter and one receiver; however, the limited range of the downlink wake-up receiver in [11] required use of a third device (the mobile phone) to close a reasonable link budget.

It should be noted that all of the described work thus far has not had any custom silicon implementations, and thus no actual low-power device has been demonstrated.

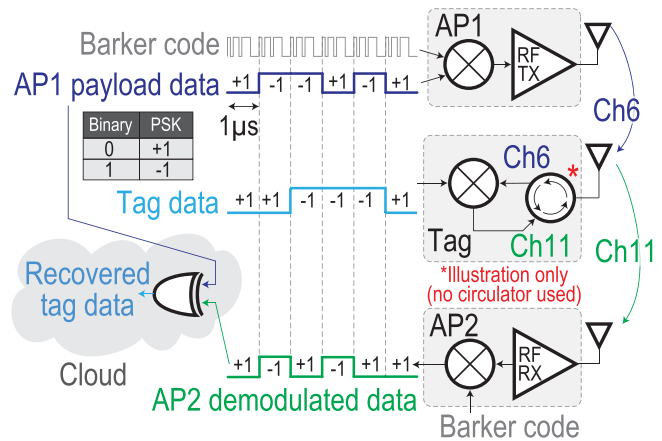


Fig. 5. BPSK-based example of how tag data is decoded in the cloud via code-word translation technique.

### C. Proposed Wi-Fi-Compatible Backscatter Approach

In this article, we adopt the idea of Hitchhike, but propose a more complete solution using two Wi-Fi APs only as shown in Fig. 4(d), while increasing the communication range with the proposed IC solution, which will be discussed in Section IV.

The main idea in Hitchhike is the code-word translation technique that enables fully Wi-Fi compliant operation, as illustrated in Fig. 5 using BPSK for simplicity. For an 802.11b Wi-Fi signal, a 1 Mbps payload data is first correlated with an 11-bit Barker code sequence for DSSS. When the payload symbol is 0, the Barker sequence is unchanged, while a payload symbol of 1 makes the phase of Barker sequence inverse. This modulated signal is then up-converted to RF, transmitted out by AP1, and incident to the tag.

At the tag side, a similar modulation method is used to modulate the tag data onto the incident signal. When the tag symbol is 0, the Wi-Fi data are unchanged, while a tag symbol of 1 makes the phase of Wi-Fi data inverse. This tag-data-modulated Wi-Fi signal is then backscattered to an alternate Wi-Fi channel for reception by AP2, noting that frequency-translation eliminates the self-jammer issue as discussed in Section II.

At AP2, the received backscattered signal is down-converted and correlated with the same 11-bit Barker code sequence used in AP1, and demodulated data is obtained—though this data is a mix between the originally transmitted packet by AP1 and the tag's data. Finally, by doing a simple XOR between the AP1 payload data and the AP2 demodulated data, the tag data can be recovered in the cloud. To make this technique work, the backscattering tag should have a wake-up receiver that is sufficiently sensitive to enable a link budget when the two Wi-Fi APs are placed 10–20 m apart, as is typically done in home- or office-based mesh networks.

## IV. BACKSCATTER TAG IMPLEMENTATION

### A. System Overview and Work Flow

To improve the downlink path of the tag compared to [11], the downlink wake-up receiver must be improved in terms of:

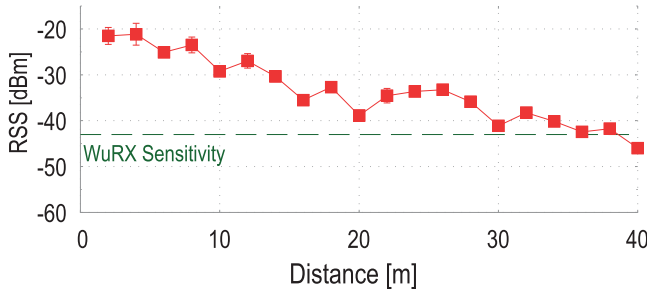


Fig. 6. Measured received power at tag location over TX-to-Tag distance.

- 1) *Low Power Consumption*: Since the downlink wake-up receiver needs to be always on such that the tag can respond immediately to packet requests, it can become the power bottleneck of the entire tag IC.
- 2) *Sufficient Sensitivity*: The sensitivity of the downlink wake-up receiver directly determines the achievable communication range between the tag IC and the incident source, so the sensitivity needs to be sufficient for the target applications. For the target IoT applications using 2.4-GHz Wi-Fi channels, a  $-40$ -dBm sensitivity is sufficient to achieve a  $>30$  m range based on RSSI over TX-to-tag distance measurements in a typical office environment as shown in Fig. 6.
- 3) *Standards Compatibility*: Before the transmitting Wi-Fi AP provides the incident signal for uplink backscattering, it is first reused to send an indication packet for the downlink wake-up receiver to tell the tag to begin backscattering at the appropriate time. Therefore, the downlink wake-up receiver also needs to be able to demodulate the indication Wi-Fi packet and distinguish this packet from other standards.

These requirements are exactly in line with recent researches targeting standard-compatible wake-up receivers [18]–[20]. Therefore, in this design a Wi-Fi-compatible wake-up receiver that leverages the idea of back-channel communication, where signals are generated by a standard-compliant transmitter, yet encode information in an auxiliary low-complexity and low data rate modality [18], is utilized.

The complete block diagram of the backscatter tag IC is depicted in Fig. 7(a). It consists of a downlink Wi-Fi-compatible wake-up receiver, an uplink transmission-line-less SSB QPSK backscatter modulator driven by a PLL as discussed in Section II, and a crystal oscillator with divider logic that provides global frequency generation.

For the downlink wake-up receiver, an energy-detection based architecture is adopted for low standby power, and therefore requires a carefully crafted wake-up packet that is Wi-Fi compatible and able to encode information that can be demodulated in an OOK fashion. Here, the transmitting Wi-Fi AP first initiates a  $107$ - $\mu$ s broadcast packet, and after a distributed interframe space (DIFS) time of  $50$   $\mu$ s, the AP sends another broadcast packet of the same  $107$   $\mu$ s length, as depicted in Fig. 7(b) shown as packets P0 and P1. These packets are built to comply with existing 802.11b protocols, and the energy valley provided by the DIFS time makes it suitable for OOK demodulation.

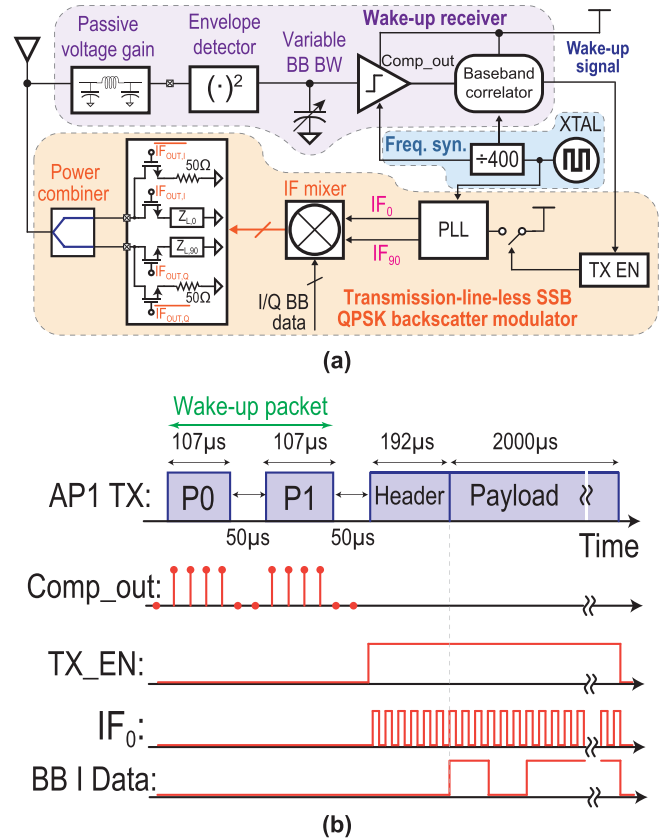


Fig. 7. Proposed backscatter-based IoT tag IC. (a) Block diagram. (b) Wake-up and backscatter timing.

The wake-up signal is first amplified and filtered by the front-end matching network that provides 8 dB of passive voltage gain, which directly improves the sensitivity of an energy-detection based RX [21]. An envelope detector (ED) then directly demodulates the RF wake-up signal to baseband via its 2nd order nonlinearity while a programmable capacitor is used at the ED output to set the bandwidth for baseband signal filtering. The ED output is then oversampled and digitized by a two-stage dynamic comparator with a programmable threshold to reduce offset voltage issues and optimize sensitivity [21]. The comparator output is then processed by an 11-bit digital correlator with soft-decision decoding to enable robust detection of the pre-specified Wi-Fi signature. Once the value exceeds a pre-defined threshold, a wake-up signal is generated.

After the wake-up event, the tag counts for a pre-specified amount of time until the uplink backscatter modulator is enabled. Before any tag data modulation starts, the  $192$ - $\mu$ s packet header is first backscattered (with frequency translation) to the receiving AP2, though without any phase alteration to ensure correct reception by AP2. After the header, the payload data is modulated by the tag data and then backscattered to AP2. Finally, AP1 and AP2 recover the tag data in cloud. The complete work flow timing of the proposed backscatter system is depicted in Fig. 7(b).

### B. Passive Pseudo-Balun Envelope Detector

Since the sensitivity of conventional energy-detection based wake-up receivers tend to be limited by the performance of

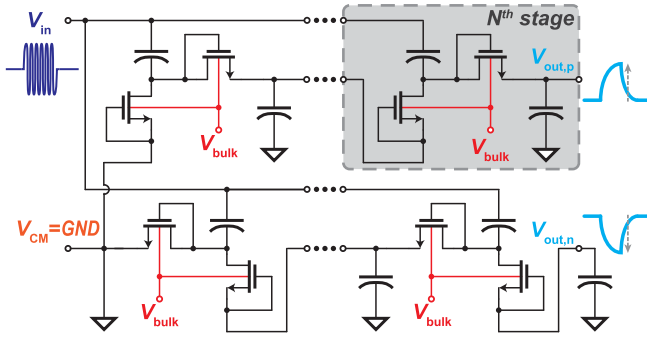


Fig. 8. Schematic of passive pseudo-balun ED.

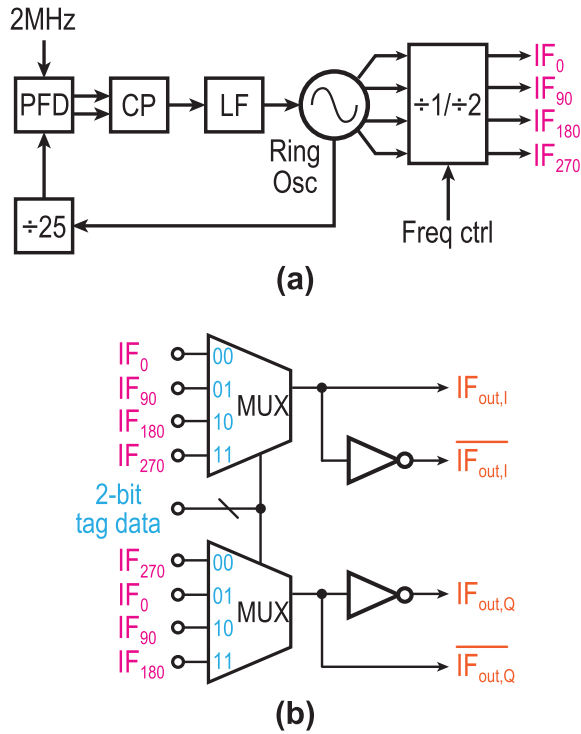
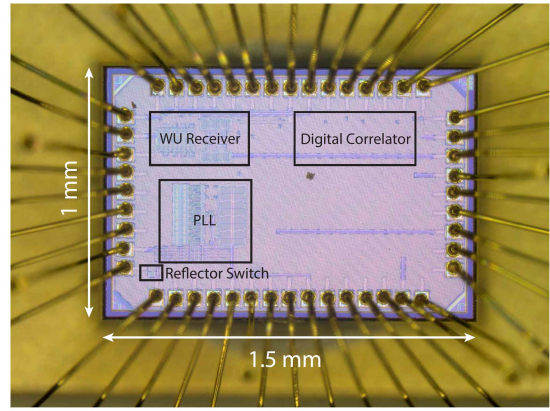


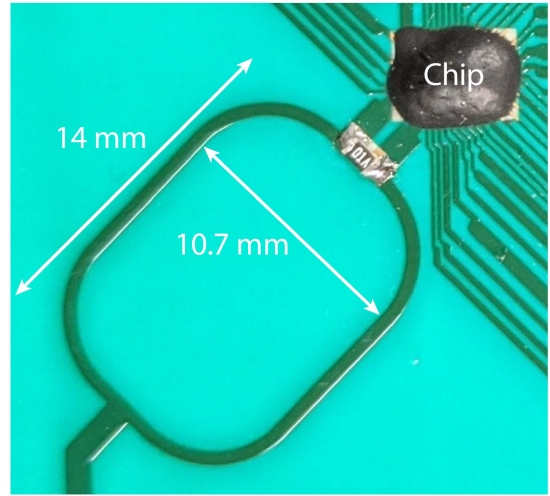
Fig. 9. Block diagram of (a) ring oscillator based integer- $N$  PLL and (b) digital SSB IF mixer.

the ED, a careful ED design is required here. To support the passive voltage gain, the ED must provide a large enough input resistance to not degrade the passive voltage gain of the front-end matching network, while provide sufficient output bandwidth for the baseband signal, in this case 200 kHz for sharp rising and falling time of the baseband signal. Active EDs [21], [22] can offer high input resistance with wide bandwidths, but this trades-off with  $1/f$  noise and power consumption. Passive EDs, on the other hand, although achieve lower input resistance compared to active EDs under same output bandwidth, do not have any  $1/f$  noise concerns and therefore permit smaller devices with lower input capacitance, which enables larger passive voltage gain [23]. Most importantly, passive EDs consume zero power. For these reasons, a passive ED is adopted in this design.

The implemented passive ED adopts a pseudo-balun architecture as shown in Fig. 8 [23]. It demodulates a single-ended



(a)



(b)

Fig. 10. (a) Micrograph of the backscatter chip. (b) Photograph of the chip assembled with the on-board Wilkinson power combiner.

input RF signal to a pseudo-differential output signal, which enables a  $2\times$  conversion gain compared to a single branch, which therefore provides 6 dB more noise rejection for the post-ED stage. Moreover, this architecture inherently provides 1.5 dB of sensitivity improvement under the same output bandwidth compared to its single-ended counterpart. To overcome  $V_t$  variation, all NMOS transistors are implemented in a deep N-well, and the bulk node is connected to a 4-bit diode ladder voltage reference that provides a tunable body-to-source substrate bias,  $V_{BS}$ , to set the output bandwidth. Based on simulation, a 100 mV increase in  $V_{BS}$  corresponds to a  $\sim 1.46\times$  increase in bandwidth in this design, and 500 mV of  $V_{BS}$  corresponds to the desired 200 kHz of output bandwidth. Following the design procedure proposed in [23], the ED stage number  $N$  is chosen to be 4 in this design to achieve the highest ED output SNR under a pre-defined bandwidth.

C. PLL and Digital SSB IF Mixer

Fig. 9(a) shows the block diagram of the PLL that drives the backscatter modulator. For the 2.4-GHz ISM band, the center frequencies of Wi-Fi channels 1, 6, and 11 are located at

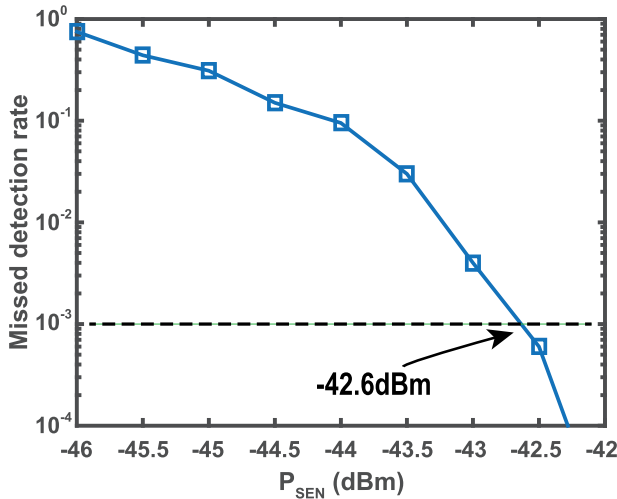


Fig. 11. Measured downlink WuRX sensitivity.

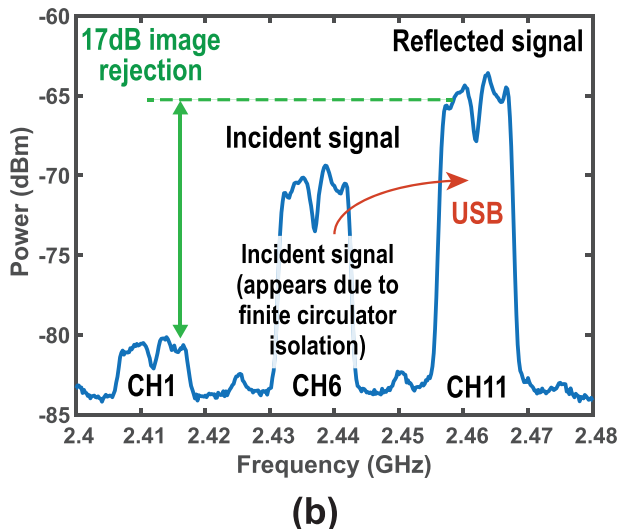
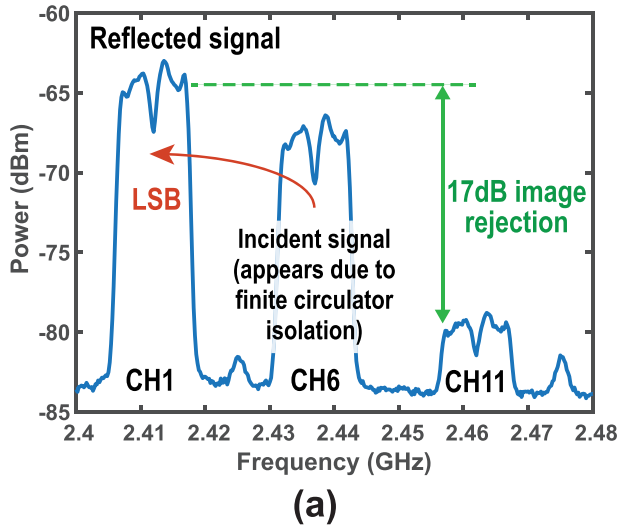


Fig. 12. Measured spectrum showing SSB backscatter-based frequency translation to (a) lower sideband and (b) upper sideband.

2412, 2437, and 2462 MHz, respectively. To backscatter to an adjacent channel, a 25-MHz IF clock is then required, while

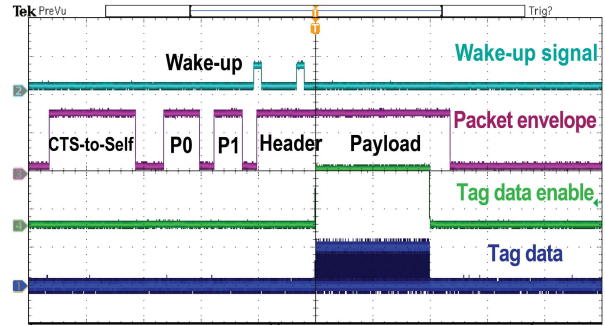


Fig. 13. Measured wake-up and backscatter timing sequence.

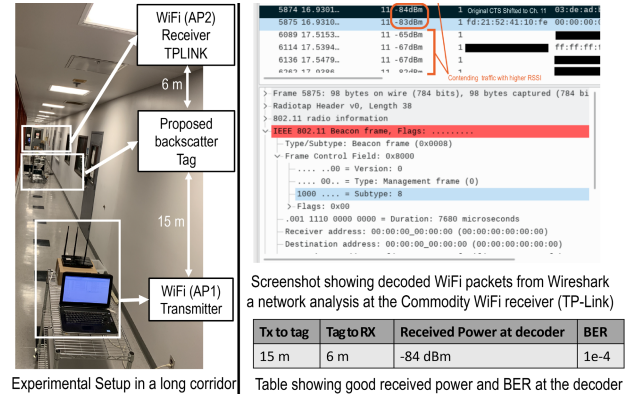


Table showing good received power and BER at the decoder

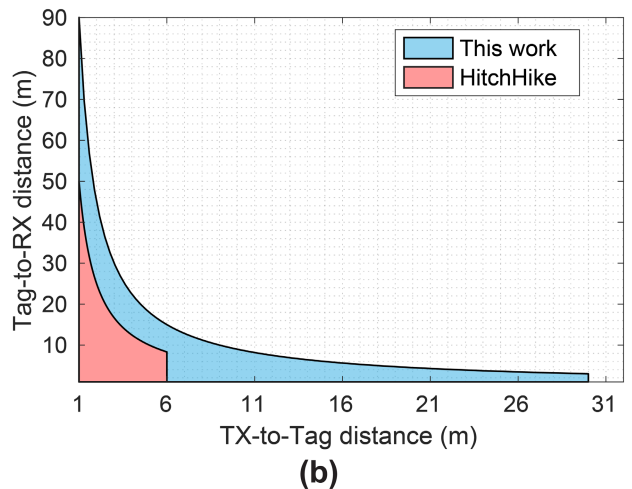


Fig. 14. Wireless over-the-air measurement (a) experimental setup and network analysis tool showing decoded backscatter packet with commodity Wi-Fi RX and (b) 5 $\times$  wake-up range and 2 $\times$  the coverage area improvement in comparison to HitchHike [11].

a 50-MHz IF clock is desired to enable translation between channels 1 and 11. Therefore, a locking frequency of 50 MHz is chosen for the PLL. With a 2-MHz frequency reference divided from the XTAL clock, a standard type-II integer- $N$  PLL is adopted with a divider ratio of 25. To provide the required quadrature IF clock for SSB backscattering, the voltage controlled oscillator (VCO) is implemented via a ring oscillator that provides the 4 clock phases. Moreover, these four phases of clocks are passed through divider logic to alternate the frequency between 25 or 50 MHz depends on the operating channels.

TABLE I  
COMPARISON WITH STATE-OF-THE-ART BACKSCATTER SYSTEMS

	[6] ISSCC'07	[7] TMTT'12	[8] JSSC'15	[9] SIGCOMM'14	[10] NSDI'16	[11] SenSys'16	This Work
<b>Technology node</b>	130 nm	No chip	65 nm	No chip	No chip	No chip	<b>65 nm</b>
<b>Chip core area</b>	0.55 mm <sup>2</sup>	No chip	0.26 mm <sup>2</sup>	No chip	No chip	No chip	<b>0.34 mm<sup>2</sup></b>
<b>Operating frequency</b>	860~960 MHz	850~950 MHz	5.8 GHz	2.4 GHz	2.4 GHz	2.4 GHz	<b>2.4 GHz</b>
<b>Range</b>	Symmetric TX-to-Tag = Tag-to-RX	7 m	4.5 m	0.1 m <sup>*</sup>	N/A	6 m	<b>10.5 m</b>
	TX-to-Tag=1 m, Tag-to-RX distance	N/A	N/A	N/A	0.65 m <sup>◊</sup>	30.5 m	<b>91 m</b>
	TX-to-Tag=15 m, Tag-to-RX distance	N/A	N/A	N/A	N/A	N/A	<b>6 m</b>
<b>Incident signal source</b>	Single-tone CW	Single-tone CW	Single-tone CW	Wi-Fi	Single-tone CW	Wi-Fi	<b>Wi-Fi</b>
<b>Reflected wave RX</b>	RFID reader	RFID reader	RFID reader	Wi-Fi	Wi-Fi	Wi-Fi	<b>Wi-Fi</b>
<b>Max data rate</b>	640 kbps	400 kbps	2.5 Mbps	1 kbps	11 Mbps	1 Mbps	<b>2 Mbps</b>
<b>Downlink wake-up range</b>	7 m	N/A	1 m	2.1 m	2.1 m	6 m	<b>&gt;30 m</b>
<b>Downlink sensitivity</b>	-14 dBm	N/A	-23 dBm	N/A	N/A	N/A	<b>-42.5 dBm</b>
<b>Downlink RX standby/wake-up power</b>	N/A	N/A	8.2 $\mu$ W	9 $\mu$ W <sup>†</sup>	18 $\mu$ W <sup>†</sup>	N/A	<b>2.8 <math>\mu</math>W</b>
<b>Uplink backscatter communication power</b>	N/A	5 $\mu$ W <sup>◊</sup>	113 $\mu$ W	0.65 $\mu$ W <sup>†</sup>	59.2 $\mu$ W <sup>‡</sup>	33 $\mu$ W <sup>‡</sup>	<b>28 <math>\mu</math>W</b>
<b>SSB Modulation?</b>	No	No	No	No	No	Off-chip	<b>On-chip</b>

\*Limited by power harvester.

◊2.1 m when using extended correlation.

†Board level designs using commercial off-the-shelf devices.

◊Measured at 400 kbps data rate.

‡Simulated values.

Fig. 9(b) shows the implementation of the digital SSB IF mixer. Two 4:1 MUX logics with 90° rotated IF clock input are used, and by controlling the MUXs via a 2-bit tag data, QPSK modulation can be achieved.

## V. MEASUREMENT RESULTS

The backscatter tag IC is fabricated in a 65-nm CMOS process, occupying a core area of 0.34 mm<sup>2</sup>. A die photograph is shown in Fig. 10(a). Although there are many possible ways to perform power combining, in this initial design, an on-board Wilkinson power combiner is implemented, as shown in Fig. 10(b).

The sensitivity waterfall curve of the downlink WuRX is shown in Fig. 11, revealing a sensitivity of -42.6 dBm for a missed detection rate (MDR) of 10<sup>-3</sup> with less than a 1/h false alarm rate. This sensitivity is sufficient to support an AP-to-tag wake-up distances of >30 m as indicated by path loss measurement shown in Fig. 6.

Wired benchtop tests with a 17-dB-isolation circulator, used for characterization purposes only, show that an incident -40-dBm 802.11b Wi-Fi signal at channel 6 (-57 dBm power shown on the spectrum analyzer due to finite circulator isolation), can be reflected to either channel 1 or 11 at -55 dBm with 17 dB of image rejection in the opposite channel, as seen in Fig. 12 for lower sideband modulation (a) and upper sideband modulation (b).

Transient waveforms in Fig. 13 shows that the tag correctly wakes up upon reception of the specially crafted yet standards-compliant Wi-Fi packets. The tag data then waits for the header to be backscattered first, and then is enabled to modulate the payload.

During wake-up mode, the chip consumes 2.8  $\mu$ W: 1.5  $\mu$ W from the crystal oscillator, and 1.3  $\mu$ W from the baseband and correlator. During active mode, the backscatter circuits consume 28  $\mu$ W, where the charge-pump consumes 10  $\mu$ W, and the digital portion of the circuits (i.e., ring oscillator, divider, phase-frequency detector (PFD), and SSB IF mixer) consume the remaining 18  $\mu$ W. The PLL phase noise at 1 MHz frequency offset is -114 dBc/Hz based on simulation. Moreover, the PLL settling time is ~5.5  $\mu$ s, which is well within the 50  $\mu$ s window between the end of the wake-up packet and the start of the header packet as shown in Fig. 7(b).

The wireless over-the-air measurement setup is shown in Fig. 14(a), where a Wi-Fi access point (AP1) transmits packets to the tag, which backscatters them to a different channel for reception by a TPLINK Archer C7 access point (AP2). For this prototype, the chip is assembled via chip-on-board, and a commercial off-the-shelf 2.4 GHz whip antenna with 3 dBi peak gain is used. For the transmitting and receiving access points, 2.4-GHz antennas with 8 dBi gain are employed on the commercial off-the-shelf hardware—these are standard antennas used in Wi-Fi routers and access points. Wireless test shows that the tag can successfully communicate at any distance between APs that are located 21 m away from each other, or to a 91 m away AP if the tag is within 1 m of any other Wi-Fi node as shown in Fig. 14(b).

Compared to the prior-art listed in Table I, this work is the first IC-based implementation of Wi-Fi backscatter, and thus, also achieves the lowest power consumption and longest range. Compared to other prior-art backscatter solutions, this work enables SSB modulation and operation without a tone-generator.

## VI. CONCLUSION

This article has presented the first backscatter IC that can communicate directly with commodity Wi-Fi transceivers. The presented design consumes only  $2.8 \mu\text{W}$  with  $-42.5\text{-dBm}$  sensitivity during down-link wake-up operation, and consumes  $28 \mu\text{W}$  with  $17\text{-dB}$  sideband rejection during uplink backscatter operation, all while maintaining full compatibility with commodity Wi-Fi hardware. Future work includes further improvement to range, operation in the 5- or 6-GHz Wi-Fi bands, and/or frequency-translation between the 2.4-GHz band and the 5/6-GHz bands (or vice versa). Regardless of future directions, the overall presented concept is a step in the right direction to enable low-cost deployment of Wi-Fi compatible tags for the next generation of low-power wireless IoT devices.

## REFERENCES

- [1] P. P. Mercier and A. P. Chandrakasan, *Ultra-Low-Power Short-Range Radios*. New York, NY, USA: Springer, 2015.
- [2] P. Laurie, "An eye on the enemy over the horizon," *New Scientist*, pp. 420–423, Nov. 1974.
- [3] U. Karthaus and M. Fischer, "Fully integrated passive uhf rfid transponder ic with  $16.7\text{-}\mu\text{w}$  minimum Rf input power," *IEEE J. Solid-State Circuits*, vol. 38, no. 10, pp. 1602–1608, Oct. 2003.
- [4] R. Glidden *et al.*, "Design of ultra-low-cost UHF RFID tags for supply chain applications," *IEEE Commun. Mag.*, vol. 42, no. 8, pp. 140–151, Aug. 2004.
- [5] W. G. Yeoh, Y. B. Choi, K. Y. Tham, S. X. Diao, and Y. S. Li, "A CMOS 2.45-GHz radio frequency identification tag IC with read/write memory," in *Proc. IEEE Radio Freq. Integr. Circuits Symp.*, Jun. 2005, pp. 365–368.
- [6] R. Barnett *et al.*, "A passive UHF RFID transponder for EPC gen 2 with  $-14\text{dBm}$  sensitivity in  $0.13\text{-}\mu\text{m}$  CMOS," in *IEEE ISSCC Dig. Tech. Papers*, Feb. 2007, pp. 582–623.
- [7] S. J. Thomas, E. Wheeler, J. Teizer, and M. S. Reynolds, "Quadrature amplitude modulated backscatter in passive and semipassive UHF RFID systems," *IEEE Trans. Microw. Theory Techn.*, vol. 60, no. 4, pp. 1175–1182, Apr. 2012.
- [8] A. Shirane *et al.*, "RF-powered transceiver with an Energy- and spectral-efficient IF-based quadrature backscattering transmitter," *IEEE J. Solid-State Circuits*, vol. 50, no. 12, pp. 2975–2987, Dec. 2015.
- [9] B. Kellogg, A. Parks, S. Gollakota, J. R. Smith, and D. Wetherall, "Wi-Fi Backscatter: Internet connectivity for RF-powered devices," in *Proc. ACM Conf. SIGCOMM*, Aug. 2014, pp. 607–618.
- [10] B. Kellogg *et al.*, "Passive Wi-Fi: Bringing low power to Wi-Fi transmissions," in *Proc. 13th USENIX Symp. Netw. Syst. Design Implement.*, Mar. 2016, pp. 151–164.
- [11] P. Zhang, D. Bharadia, K. Joshi, and S. Katti, "HitchHike: Practical backscatter using commodity WiFi," in *Proc. ACM Conf. Embedded Netw. Sensor Syst. (SenSys)*, Nov. 2016, pp. 259–271.
- [12] S. O'Driscoll *et al.*, "A  $200\text{-}\mu\text{m} \times 200\text{-}\mu\text{m} \times 100\text{-}\mu\text{m}$ ,  $63\text{nW}$ ,  $2.4\text{GHz}$  injectable fully-monolithic wireless bio-sensing system," in *Proc. IEEE Radio Freq. Integr. Circuits Symp. (RFIC)*, Jun. 2017, pp. 256–259.
- [13] V. W. Leung *et al.*, "A CMOS distributed sensor system for high-density wireless neural implants for brain-machine interfaces," in *Proc. IEEE 44th Eur. Solid State Circuits Conf. (ESSCIRC)*, Sep. 2018, pp. 230–233.
- [14] P.-H.-P. Wang, C. Zhang, H. Yang, D. Bharadia, and P. P. Mercier, "20.1 A  $28\text{-}\mu\text{W}$  IoT tag that can communicate with commodity WiFi transceivers via a Single-Side-Band QPSK backscatter communication technique," in *IEEE ISSCC Dig. Tech. Papers*, Feb. 2020, pp. 312–314.
- [15] D. Bharadia, E. McMillin, and S. Katti, "Full duplex radios," in *Proc. ACM SIGCOMM*, Aug. 2013, pp. 375–386.
- [16] B. Razavi, "A  $900\text{-MHz}/1.8\text{-GHz}$  CMOS transmitter for dual-band applications," *IEEE J. Solid-State Circuits*, vol. 34, no. 5, pp. 573–579, May 1999.
- [17] B. Razavi, *RF Microelectronics*, 2nd ed. Upper Saddle River, NJ, USA: Prentice-Hall, 2011.
- [18] N. E. Roberts *et al.*, "26.8 A  $236\text{nW}$   $-56.5\text{dBm}$ -sensitivity Bluetooth low-energy wakeup receiver with energy harvesting in  $65\text{nm}$  CMOS," in *IEEE ISSCC Dig. Tech. Papers*, Jan. 2016, pp. 450–451.
- [19] P.-H.-P. Wang and P. P. Mercier, "28.2 A  $220\text{-}\mu\text{W}$   $-85\text{dBm}$  sensitivity BLE-compliant wake-up receiver achieving  $-60\text{dB}$  SIR via single-die Multi-channel FBAR-based filtering and a 4-Dimensional wake-up signature," in *IEEE ISSCC Dig. Tech. Papers*, Feb. 2019, pp. 440–442.
- [20] P.-H.-P. Wang and P. P. Mercier, "A  $4.4\text{-}\mu\text{W}$   $-92\text{--}90.3\text{dBm}$  sensitivity dual-mode BLE/Wi-Fi wake-up receiver," in *Proc. IEEE Symp. VLSI Circuits*, Jun. 2020, pp. 1–2.
- [21] P.-H.-P. Wang *et al.*, "A near-zero-power wake-up receiver achieving  $-69\text{-dBm}$  sensitivity," *IEEE J. Solid-State Circuits*, vol. 53, no. 6, pp. 1640–1652, Jun. 2018.
- [22] P.-H.-P. Wang *et al.*, "A  $400\text{MHz}$   $4.5\text{nW}$   $-63.8\text{dBm}$  sensitivity wake-up receiver employing an active pseudo-balun envelope detector," in *Proc. 43rd IEEE Eur. Solid State Circuits Conf. ESSCIRC*, Sep. 2017, pp. 35–38.
- [23] P.-H.-P. Wang *et al.*, "A  $6.1\text{-nW}$  wake-up receiver achieving  $-80.5\text{-dBm}$  sensitivity via a passive pseudo-balun envelope detector," *IEEE Solid-State Circuits Lett.*, vol. 1, no. 5, pp. 134–137, May 2018.



**Po-Han Peter Wang** (Member, IEEE) received the B.S. degree in electrical engineering from National Taiwan University (NTU), Taipei, Taiwan, in 2011, and the M.S. and Ph.D. degrees in electrical and computer engineering from the University of California at San Diego (UCSD), La Jolla, CA, USA, in 2014 and 2019, respectively.

In 2013, he was an RFIC Design Intern with Broadcom Corporation, San Diego, CA. He is currently an RFIC Design Engineer with Broadcom Inc., San Diego. His research interests include the design of energy-efficient transceiver for wireless communications, reconfigurable RF front ends and filters, and ultralow-power mixed-signal circuits.



**Chi Zhang** received the B.E. degree from the School of Optical and Electronic Information, Huazhong University of Science and Technology, Wuhan, China, in July 2013, and the Ph.D. degree from the Department of Electrical and Computer Engineering, University of Wisconsin-Madison, Madison, WI, USA, in December 2017.

He was a Post-Doctoral Scholar with the University of California at San Diego, San Diego, CA, USA, from March 2018 to January 2019 and from July 2019 to November 2019. His research interests include low-power and ubiquitous sensing, Internet-of-things, low-power wireless networking, and scalable wireless power delivery.



**Hongsen Yang** (Graduate Student Member, IEEE) received the B.S. degree in electrical and computer engineering from the University of Illinois at Urbana-Champaign (UIUC), Urbana, IL, USA, in 2017, and the M.S. degree in electrical and computer engineering from the University of California at San Diego (UCSD), La Jolla, CA, USA, in 2019.

He is currently a Junior RF Engineer with Aethercomm, Inc., San Diego, CA. His research interests include RF front ends, power amplifiers, and human body communication systems.



**Manideep Dunna** received the B.Tech. and M.Tech. degrees (Hons.) from IIT Madras, Chennai, India, in 2017 and 2018, respectively. He is currently pursuing the Ph.D. degree with the University of California at San Diego (UCSD), La Jolla, CA, USA, with the WCSNG Research Group.

His research focuses on using backscatter techniques for low power wireless relays.

Mr. Dunna is a recipient of the Charles Lee Powell fellowship at UCSD.

**Dinesh Bharadia**, photograph and biography not available at the time of publication.



**Patrick P. Mercier** (Senior Member, IEEE) received the B.Sc. degree in electrical and computer engineering from the University of Alberta, Edmonton, AB, Canada, in 2006, and the S.M. and Ph.D. degrees in electrical engineering and computer science from the Massachusetts Institute of Technology (MIT), Cambridge, MA, USA, in 2008 and 2012, respectively.

He is currently an Associate Professor in electrical and computer engineering with the University of California at San Diego (UCSD), La Jolla, CA, USA, where he is also the Co-Director of the Center for Wearable Sensors. His research interests include the design of energy-efficient microsystems, focusing on the design of RF circuits, power converters, and sensor interfaces for miniaturized systems and biomedical applications.

Dr. Mercier is currently a member of the ISSCC International Technical Program Committee, the CICC Technical Program Committee, the VLSI Symposium Technical Program Committee. He received the Natural Sciences and Engineering Council of Canada (NSERC) Julie Payette Fellowship in 2006, the NSERC Postgraduate Scholarships in 2007 and 2009, an Intel Ph.D. Fellowship in 2009, the 2009 IEEE International Solid-State Circuits Conference (ISSCC) Jack Kilby Award for Outstanding Student Paper at ISSCC 2010, the Graduate Teaching Award in Electrical and Computer Engineering at UCSD in 2013, the Hellman Fellowship Award in 2014, the Beckman Young Investigator Award in 2015, the DARPA Young Faculty Award in 2015, the UC San Diego Academic Senate Distinguished Teaching Award in 2016, the Biocom Catalyst Award in 2017, the NSF CAREER Award in 2018, a National Academy of Engineering Frontiers of Engineering Lecture in 2019, and the San Diego County Engineering Council Outstanding Engineer Award in 2020. He has served as an Associate Editor for the IEEE TRANSACTIONS ON VERY LARGE SCALE INTEGRATION (TVLSI) from 2015 to 2017. Since 2013, he has served as an Associated Editor for the IEEE TRANSACTIONS ON BIOMEDICAL CIRCUITS AND SYSTEMS (TBioCAS). He is an Associate Editor of IEEE SOLID-STATE CIRCUITS LETTERS. He was the coeditor of *Ultralow-Power Short Range Radios* (Springer, 2015), *Power Management Integrated Circuits* (CRC Press, 2016), and *High-Density Electrocortical Neural Interfaces* (Academic Press, 2019).